Available online at www.sciencedirect.com
ScienceDirect
Journal of Fluorine Chemistry 129 (2008) 402–408
JOURNAL OF FLUORINE CHEMISTRY
www.elsevier.com/locate/fluor

Synthesis, structure and spectral study of two types of novel fluorescent BF_2 complexes with heterocyclic 1,3-enaminoketone ligands

Min Xia [a,b,*], Bin Wu [a], Guofeng Xiang [a]

[a] *Department of Chemistry, Zhejiang Sci-Tech University, Hangzhou 310018, PR China*
[b] *Key Laboratory of Advanced Textile Materials and Manufacturing Technology(Ministry of Education), Zhejiang Sci-Tech University, Hangzhou 310018, PR China*

Received 1 November 2007; received in revised form 30 January 2008; accepted 31 January 2008
Available online 10 March 2008

Abstract

Two types of novel BF_2 complexes are readily obtained by the reaction of BF_3OEt with 3-(2-oxo-2-arylethylidene)-3,4-dihydro-1*H*-quinoxalin-2-ones or 3-(2-oxo-2-arylethylidene)-3,4-dihydrobenzo[1,4]oxazin-2-ones, respectively in refluxing acetic acid/toluene solvent mixture. The complexes are confirmed by elemental analysis, FT-IR, ^{1}H, ^{13}C, ^{11}B, ^{19}F NMR and one of them is executed its X-ray crystallographic study. The outstanding photophysical properties of these complexes are determined by UV–vis absorption and fluorescence emission spectroscopy.

Keywords: BF_2 complex; Heterocyclic 1,3-enaminoketone; Fluorescence; X-ray crystallography

1. Introduction

Organic difluoroboron complexes are well-known fluorescent molecules with high fluorescence intensity and quantum yields which are widely used in many applications such as photo-dynamic cancer treatment, laser dyes, biological fluoroprobes, fluorescent indicators and photo sensitizers as well. There are two main types of these complexes, classified as N, N double-dentate and O, O double-dentate compounds, BODIPY (boradipyrromethene) [1–4] and 1,3,2-dioxaborine [5–8] are their corresponding representatives. However, there are few reports [9–11] available on the generation of difluoroboron complexes with N, O double-dentate ligands. Although we have reported [12] the synthesis and X-ray crystallography of a difluoroboron complex containing the N, O double-dentate ligand derived from a Schiff's base of salicyaldehyde, its poor quantum yield and low fluorescence intensity compelled us to explore other approaches to such compounds.

1,3-Enaminoketones, the isosteric analogues to 1,3-enolic ketones, are excellent candidates as N, O double-dentate ligands to form 1,3,2-oxazaborines which are supposed to have photophysical properties similar to those of 1,3,2-dioxaborines derived from 1,3-diketones. In spite of the report [9] from Itoh et al. on the preparation of some examples of 1,3-enaminoketonatoboron difluorides, their UV absorption peaks were limited to less than 350 nm and their fluorescence emissions were unable to be detected by human eyesight, due to the small conjugations contributed by their simple 1,3-enaminoketone ligands. In order to obtain some 1,3,2-oxazaborine difluorides with remarkable fluorescence intensity for direct observation by human eyesight, the arrangement of 1,3-enaminoketone structures into heterocycles should be an effective route, since rigid skeletons and large electron densities of heterocycles will dramatically promote the fluorescence property of a given molecule.

3-(2-Oxo-2-arylethylidene)-3,4-dihydro-1*H*-quinoxalin-2-ones and 3-(2-oxo-2-arylethylidene)-3,4-dihydrobenzo[1,4]oxazin-2-ones are two heterocycles in which 1,3-enaminoketones can be inserted into their molecular structures. Fortunately, the BF_2 complexes generated from these two heterocyclic 1,3-enaminoketones are novel compounds with intensively yellowish green fluorescence. To the best of our knowledge, there has been no report to date in the literature on the synthesis of such 1,3,2-oxazaborine difluorides containing heterocyclic 1,3-enaminoketones. Herein we describe our preparation of these BF_2 complexes as well as the confirmation of their molecular

* Corresponding author. Tel.: +86 571 86843224; fax: +86 571 88802212.
E-mail address: xiamin@hzcnc.com (M. Xia).

0022-1139/$ – see front matter
doi:10.1016/j.jfluchem.2008.01.019

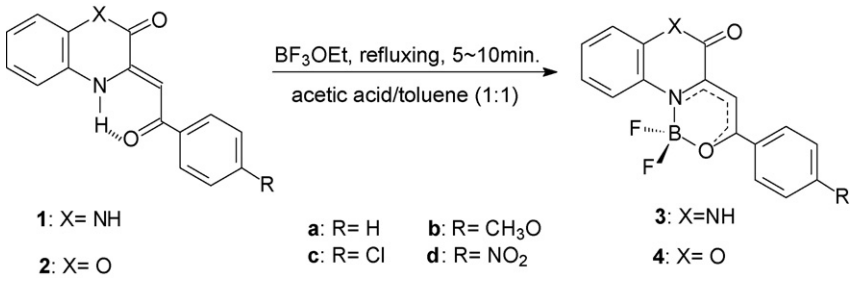

Scheme 1.

structures and the measurements of their photophysical properties.

2. Results and discussion

2.1. Synthesis of complexes *3a–d* and *4a–d*

The two types of BF_2 complexes, i.e. 3-(2-oxo-2-arylvinyl)-1*H*-quinoxalinonatoboron difluorides **3a–d** or 3-(2-oxo-2-arylvinyl)benzo[1,4]oxazinonatoboron difluorides **4a–d**, can both be readily prepared by the reaction of the corresponding 3-(2-oxo-2-arylethylidene)-3,4-dihydro-1*H*-quinoxalin-2-ones **1a–d** or 3-(2-oxo-2-arylethylidene)-3,4-dihydrobenzo[1,4]oxazin-2-ones **2a–d** with 5 eq. BF_3OEt in a refluxing acetic acid/toluene (1:1) solvent mixture for 5 min (Scheme 1). The chelations occur rapidly, when BF_3OEt is dropped into the slightly boiling solutions of **1a–d** or **2a–d** in acetic acid/toluene, the yellow solutions immediately turn dark red. After slowly cooling to room temperature, powders or crystals are precipitated from the liquors. Generally, the resulting complexes are pure enough for their subsequent spectral measurements, and the further recrystallized ones from acetic acid/toluene (1:1) can be utilized for the elemental analysis.

2.2. Solid-state studies

2.2.1. X-ray crystallography

In the solid state, X-ray crystallographic data can generally provide detailed and conclusive structural information for a given molecule. An example of complex **4b** is accordingly chosen for its crystallographic analysis; the corresponding data and structure refinement are listed in Table 1. It is clearly shown (Fig. 1) that the chelating ring formed by the six atoms is planar, and the three fused cycles involving benzo[1,4]oxazinone are also in the same plane, because the mean deviation of the three-cycle plane is much small in 0.0239 Å. The structural distortion of this complex is dramatically prohibited by the generation of the chelating ring, and this is one of the most significant reasons for its intensive fluorescence.

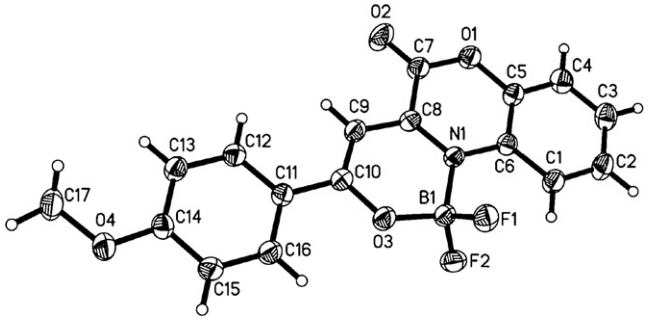

Fig. 1. The molecular structure of complex **4b**.

Due to the chelation effect, the electrons on the chelating ring are largely delocalized. Such a conclusion can be drawn independently by examining the bond lengths of C_{10}–O_3, C_{10}–C_9, C_9–C_8, C_8–N_1, B_1–O_3 and B_1–N_1 (Table 2). Comparing C_{10}–O_3 (1.319 Å), C_{10}–C_9 (1.373 Å), C_9–C_8 (1.383 Å) and C_8–N_1 (1.337 Å) bond lengths with those standard C–O (1.43 Å), C=O (1.20 Å), C–C (1.54 Å), C=C (1.34 Å), C–N (1.47 Å) and C=N (1.28 Å) distances [14], it is ready to find that these lengths are approximately equal to the averaged bond distances of the corresponding single and double bond standard lengths, especially the bond distances of C_{10}–C_9 and C_9–C_8, they are considerably close to that of an aromatic C=C (1.40 Å) bond

Table 1
Crystal data and structure refinement for complex **4b**

Empirical formula	$C_{17}H_{12}BF_2NO_4$
Formula weight	343.09
Temperature	293(2) K
Wavelength	0.71073 Å
Crystal system, space group	Monoclinic, $P2_1/n$
Unit cell dimensions	$a = 7.0534(14)$ Å $\alpha = 90°$.
	$b = 13.649(3)$ Å $\beta = 95.50(3)°$.
	$c = 15.905(3)$ Å $\gamma = 90°$.
Volume	1524.2(5) Å^3
Z, calculated density	4, 1.495 Mg/m^3
Absorption coefficient	0.121 mm^{-1}
F (0 0 0)	704
Crystal size	0.40 mm × 0.20 mm × 0.11 mm
θ Range for data collection	3.06–25.20°.
Limiting indices	$-8 \le h \le 8$, $-16 \le k \le 16$, $-19 \le l \le 19$
Reflections collected/unique	11741/2724 [R(int) = 0.0302]
Completeness to $\theta = 25.20$	98.8%
Absorption correction	Semi-empirical from equivalents
Maximum and minimum transmission	0.981 and 0.965
Refinement method	Full-matrix least-squares on F^2
Data/restraints/parameters	2724/0/228
Goodness-of-fit on F^2	1.036
Final R indices [$I > 2\theta(I)$]	$R_1 = 0.0399$, $wR_2 = 0.1131$
R indices (all data)	$R_1 = 0.0673$, $wR_2 = 0.1280$
Extinction coefficient	0.0067(15)
Largest diff. peak and hole	0.211 and −0.210 e Å^{-3}

Table 2
Selected bond lengths and bond angles of complex **4b**

Bond length (Å)		Bond angle (°)	
N_1–B_1	1.575(3)	B_1–N_1–C_8	119.20(17)
B_1–O_3	1.458(3)	N_1–B_1–O_3	110.42(17)
N_1–C_8	1.337(2)	B_1–O_3–C_{10}	126.54(17)
C_9–C_{10}	1.373(3)	O_3–C_{10}–C_9	119.36(19)
C_8–C_9	1.383(3)	N_1–C_8–C_9	122.78(19)
C_{10}–O_3	1.319(2)	C_8–C_9–C_{10}	121.53(19)
B_1–F_1	1.380(3)	F_1–B_1–F_2	110.38(18)
B_1–F_2	1.378(3)	F_1–B_1–O_3	108.92(19)
C_{11}–C_{10}	1.450(3)	F_2–B_1–N_1	109.44(18)
C_7–C_8	1.493(3)	C_6–N_1–B_1	120.96(16)
C_6–N_1	1.409(3)	F_1–B_1–N_1	108.69(18)
C_5–O_1	1.388(2)	C_7–C_8–C_9	116.88(18)
C_7–C_8	1.493(3)	C_{11}–C_{10}–O_3	115.57(18)
C_7–O_1	1.345(2)	O_3–B_1–F_2	108.98(19)
C_7–O_2	1.193(3)		

length. In addition, the isotropic displacement parameters of each atoms (0.040 $Å^2 \leq U_{iso} \leq 0.081$ $Å^2$), especially that of O_3 atom (U_{iso} = 0.053 $Å^2$), are small enough. This indicates that a single resonance structure with the large electron delocalization on the chelating ring instead of a mixed BF_2 complex with two tautomeric configurations (i.e. 1,3-ketoamine and 1,3-enolimine) is adopted in the solid state of this complex, since the obviously increased isotropic displacement parameters of partial atoms to more than 0.2 $Å^2$ will occur an out-of-order X-ray structure. Hence, the positive charge generated from the chelation is completely dispersed on O_3, N_1, C_8, C_9 and C_{11} atoms rather than localized on N_1 or even O_3 atom. Moreover, it is shown that the B_1–O_3 and B_1–N_1 distances are 1.458 and 1.575 Å respectively, they are either stretched or contracted from the corresponding standard B–O (1.34–1.40 Å) and B–N (1.61 Å) bond lengths, therefore the BF_2 group is clearly off-center from the O_3–N_1 axis. Besides, the dihedral angle (3.7°) between the C_{11}–C_{16} plane and the C_1–C_{10} plane is so small that the C_{11}–C_{16} cycle is considerably conjugated with the chelating ring. This conjugation can lead to the contracted C_{10}–C_{11} distance in 1.450 Å; it is comparatively close to an aromatic C=C (1.40 Å) rather than an ideal C–C (1.54 Å) length. The C_7–O_2 distance (1.193 Å) is equal to a standard C=O bond length, this manifests that the carbonyl group cannot take the role of a bridge to connect the C_1–C_6 cycle and the chelating ring in the conjugative pattern. However, its existence makes the great contribution to the rigidity of the BF_2 complex. Therefore, compared to those 1,3,2-oxazaborine difluorides in Itoh′s cases, our BF_2 complexes with the intensive yellowish green fluorescence and the remarkable red shifts (generally more than 100 nm) of the UV–vis absorption peaks should be attributed to the extensively conjugated region, the high degree of electron delocalization and the improved structural rigidity caused by the use of heterocyclic ligands.

2.2.2. IR spectra

Due to the extensive electron delocalization throughout the five-atom region on the chelating ring, the N_1–C_8 bond is dramatically strengthened and it remarkably exhibits the characteristic of a N=C bond, whereas the property of a C=O bond is obviously weakened for the C_{10}–O_3 bond. The peaks within 1511–1618 cm^{-1}, which are the strongest ones of these BF_2 complexes in their IR spectra, can be attributed to the vibrations of the strengthened N_1–C_8 and the weakened C_{10}–O_3 bond. The exclusion of ester or amide carbonyl group from its conjugation with other atoms can be further testified by the fact that the absorption peaks of them between the BF_2 complexes and the parent ligands are hardly shifted, it is located at ~1685 or ~1755 cm^{-1}, respectively. Moreover, the strong absorptions within 1344–1392 cm^{-1} can also be accounted for the successful chelations of BF_2 group with N, O-double dentates, since the absorptions in this range is the characteristic band of the B–O or B–N bond.

2.3. Solution-state studies

2.3.1. NMR spectra

Due to the chelations of BF_2 group with N, O-double dentates, the most obvious and significant changes in ^1H NMR spectra of BF_2 complexes are the disappearance of the signals for the intramolecular hydrogen bonds in the lowest field. Due to the heavy electron delocalization on the chelating ring, the electronic cloud adjacent to the C_9 atom considerably take part in the conjugation with its neighboring atoms, resulting the largely decreased electronic density around H_9 atom. In a ^1H NMR experiment, the decreased electronic density is manifested as the chemical shifts toward the lower field. Therefore, a noticeable down-field shift of H_9 signal can be observed from 6.70–7.00 ppm in the parent ligands to 7.18–7.39 ppm in the BF_2 complexes. In addition, compared the signals of aromatic protons in BF_2 complexes with those in ligands, it is evident that they are also moved toward down fields to a recognizable degree after the chelations.

The signal of C_{10} occurs a large high-field shift, this is the most attractive variation between the ^{13}C NMR spectra of the BF_2 complex and that of its corresponding ligand. Due to the great electron delocalization among the five atoms on the chelating cycle, C_{10} atom is endowed a high electronic density, leading to the strengthened shielding effect in such position. Hence, the signals of C_{10} are reduced from 185–191 ppm in the ligands to 164–172 ppm in the complexes. In comparison of the signals for amide or ester carbonyl groups in the BF_2 complexes and their corresponding parent ligands, little shifts can be detected, they are approximately centered at 153 ppm. This observation further indicates that the amide or ester carbonyls are isolated from the regions with the electron delocalizations.

In the ^{11}B NMR spectra, the signals of boron atoms in the complexes are limited to 2.40–2.89 ppm region, which is the typical chemical shift range of tetra-coordinated boron atoms [14]. Since the ^{11}B NMR measurements are made without employing ^{19}F decoupling, the signals of boron atoms are recognizably divided into triple peaks by the neighboring fluorine atoms. The chemical shifts of the fluorine resonance for the BF_2 complexes are listed in Table 3. There is an excellent relationship between the chemical shifts and the electronic effect of the substituents in both complexes **3** and **4**. As the

Table 3
The absorption and fluorescence spectral properties and ^{19}F chemical shifts of complexes **3a–d** and **4a–d**

Complex	λ_{abs} (nm)[a,d]	ε[c] (M^{-1} cm^{-1}) × 10^4	λ_{em} (nm)[a]	ϕ_F[b]	δ (ppm) in ^{19}F NMR
3a	416.2, 440, 467.4	4.18	481, 512	0.641	−122.92
3b	423.8, 448, 476.4	4.91	488.6, 520.6	0.672	−123.53
3c	420, 444.2, 471	3.28	487, 518	0.869	−122.88
3d	432.4, 456.2	2.61	513.5	0.633	−122.48
4a	422.4, 442.8, 468.8	3.00	493, 522.5	0.803	−123.35
4b	454.4, 481.6	3.84	509	0.593	−124.02
4c	425.4, 445.2, 469.8	2.75	496.5, 525.5	0.837	−123.27
4d	432.6, 451.8	2.45	506.5, 531	0.770	−122.85

[a] Absorption (1 μM) and fluorescence (0.08 μM) spectra at room temperature in THF solutions.
[b] Absolute fluorescence quantum yields measured with naphthacene [$\phi_F = 0.6$ ($\lambda_{ex} = 443$ nm)] as the standard.
[c] Referenced to the molar extinction coefficient of the peak with the strongest absorption.
[d] Underlined wavelengths are the peaks with the strongest absorption.

substituent is changed from an electron-donating to an electron-withdrawing group, the electron density around fluorine atom is slightly decreased, which leads to a tiny down-field chemical shift. For the complexes with the same substituted aromatic cycle, it is found that there are slight down-field shifts from the complexes **3** to the complexes **4**. Compared to the chemical shifts of fluorine atoms in Itoh′s report [9] in which signals were limited at −138.5 to −138.9 ppm, a considerable down-field shift can be observed in our case, this may be induced by the high-degree conjugation on the chelating ring in our complexes. Unlike the Itoh′s case in which two doublets with 1:1:1:1 areas were detected, the fluorine signals in our complexes are doublets with 1:1 integrals. This indicates the dihedral angle between the chelating ring and the substituted aromatic cycle is so small that the two fluorine atoms exist in the same molecular environment and they are simply split by the neighboring boron atoms. This conclusion is also testified by the X-ray crystallography of example **4b**. Besides, the B–F coupling constants in our BF_2 complexes are in 26.3–30.0 Hz, which lie between those in the Itoh′s complexes (17.1–17.9 Hz) and those in the dimmers of diethylaminodifluoroborane (42 Hz) [15].

2.3.2. *UV–vis and fluorescence spectra*

The UV–vis and fluorescence spectra of complexes **3a–d** and **4a–d** are measured and the results are listed in Table 3. Clearly, these BF_2 complexes display bright and intensive yellowish green fluorescence [see the picture in the Graphical abstract where the photo of **3b** (in the left) and **4b** (in the right) in THF solutions under the radiation at a wavelength of 254 nm is shown). These BF_2 complexes typically exhibit three UV–vis absorption bands and two fluorescence emission peaks. In some cases, however, the spectral bands are simplified into two absorption peaks and one emission peak. In general, there are good mirror symmetries between the absorption and the emission peaks (Fig. 2), the Stocks shifts are around 50 nm. Evidently, either an electron-donating or an electron-withdrawing group on the substituted aromatic cycle makes the absorption and the emission maxima with a notable red shift. This is caused by a reduced energy gap between the S_0 ground state and the S_1 excited state of a given complex, since the energy of the HOMO may well be raised more than that of the LUMO by an electron donor while the energy of the LUMO may well be lowered more than that of the HOMO by an electron acceptor. For both the absorption and the emission bands, a remarkable long-wavelength shift can be readily observed from complexes **3** to **4** in case that their aromatic substituents are the same. For these two types of complexes, an excellent correlation is established between the molar extinction coefficient (ε) and the electronic effect of the substituents. In either of them, the ε value is noticeably diminished as the substituent is varied from a donor to an acceptor. This may be attributed to the different electron densities in the conjugative regions caused by the substituents. For example, an electron-donating group can largely increase the above mentioned electronic density, resulting the enhanced transition probability of the conjugative electrons and the corresponding ε value. The opposite effect will accordingly be observed by an electron-withdrawing group. Furthermore, the ε values are reduced from complexes **3** to **4** when they have the same substituted aromatic cycle. We attribute this observation to the lower electronegativity of the N atom than that of the O atom, which leads to the enhanced transition probability of the conjugative electrons caused by the amide moiety. Although there are no specific relationships between the structures and the absolute quantum

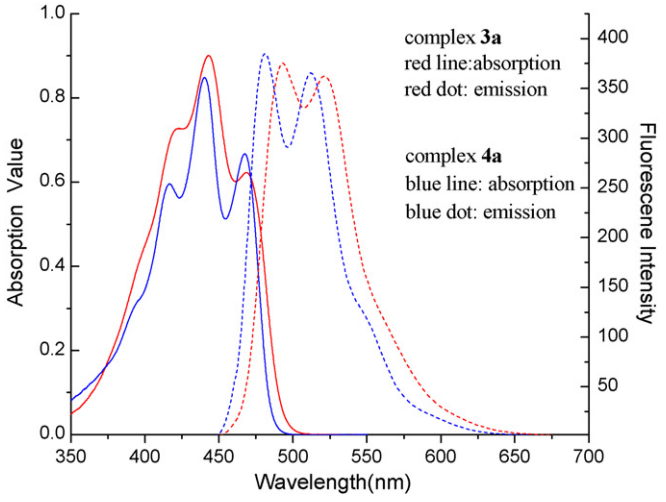

Fig. 2. Absorption and fluorescence spectra of complex **3a** and **4a** in THF solutions.

Table 4
Solvent effect on the absorption and the fluorescence properties for complex **3b**

Solvent	λ_{abs} (nm)[a]	λ_{em} (nm)[b]	ϕ/ϕ_{THF}
Benzene	481.9, 451.8, 426.9	491.6, 524	0.976
$CHCl_3$	482.5, 452.1, 426.8	494.5, 524.7	1.012
Et_2O	474, 445.3, 421.4	484, 515.6	1.005
THF	476.4, 448, 423.8	488.6, 520.6	1.000
EtOAc	474.4, 445.6, 422	486.7, 517.8	0.875
$(CH_3O)_2O$	475.4, 446.8, 423.3	489.8, 522	0.942
MeCN	474.8, 444.6, 422.8	490, 519.6	0.925
MeOH	474.2, 444, 420.2	489.7, 519	0.931

[a] Absorption values are controlled within 0.6–0.8 unit.
[b] Fluorescence intensity are controlled within 500–700 unit.

yields (Φ_F), these complexes are still worthy to be developed as the useful fluorescence materials.

Complex **3b** is selected as a sample for determining the solvent effect on its photophysical property (Table 4). It is apparent that the solvent polarity has only a slight impact on the peak wavelengths in both the absorption and the emission spectra. When **3b** is treated with polar solvents, its peaks of the absorption and the emission take place the blue shifts, such a trend is similar to that reported by Itoh [9] in their study of 1,3,2-oxazaborine difluorides with simple 1,3-enaminoketones.

3. Conclusion

Herein we describe the synthesis, structure and spectral research of two types of novel BF_2 complexes with 3-(2-oxo-2-arylethylidene)-3,4-dihydro-1*H*-quinoxalin-2-ones or 3-(2-oxo-2-arylethylidene)-3,4-dihydrobenzo[1,4]oxazin-2-ones as their heterocyclic 1,3-enaminoketone ligands. The chelations can be accomplished readily and smoothly to afford the desired complexes in excellent yields. For these BF_2 complexes, the large-span red shifts of UV–vis absorption peaks and intensive fluorescence are caused by the considerable conjugations between the chelating rings and the aromatic cycles. The data of IR, NMR and X-ray crystallography assist in elucidating the relationship between the molecular structures and the photophysical properties. The research on development of them as potential fluorescence materials will be reported in due course.

4. Experimental

4.1. Instrumentation and materials

All the compounds used are analytical reagents and some chemicals are further purified by recrystallization or distillation. Melting points are determined on a X-4 micro melting instrument and the thermometer is uncorrected. The ^{1}H NMR (400 MHz), ^{13}C NMR (100 MHz), ^{11}B NMR (128 MHz) and ^{19}F NMR (376 MHz) spectra are obtained on a Bruker Avance II DMX400 spectrometer using DMSO-d_6 as the solvent. The ^{1}H NMR and ^{13}C NMR experiments are carried out using trimethylsilane as the internal standard while the ^{11}B NMR and ^{19}F NMR spectra are recorded using BF_3OEt (0 ppm) and CF_3COOH (76.5 ppm) as the external standards, respectively. FT-IR spectra are performed as KBr pellets on a Nicolet Avatar spectrophotometer. X-ray crystallographic data is collected on a Rigaku RAXIS-RAPID apparatus. The absorption spectra are measured on a Shimadzu UV 2501(PC)S UV–vis spectrometer and the fluorescence spectra are measured on a PerkinElmer LS55 spectrophotometer. The elemental analysis is achieved on a PerkinElmer 2400 microanalyser. 3-(2-oxo-2-arylethylidene)-3,4-dihydro-1*H*-quinoxalin-2-ones (**1a–d**) and 3-(2-oxo-2-arylethylidene)-3,4-dihydro-benzo[1,4]oxazin-2-ones (**2a–d**) are prepared according to the literature [13]. The absolute quantum yields are measured using naphthacene (Φ_F = 0.6, λ_{ex} = 443 nm) as a standard and its Φ_F deviation within 440–456 nm is less than 7% in our experiments.

4.2. Synthesis of 3-(2-oxo-2-arylvinyl)-1H-quinoxalinonatoboron difluorides (3a–d) and 3-(2-oxo-2-arylvinyl)benzo[1,4] oxazinonatoboron difluorides (*4a–d*)

At room temperature, 3-(2-oxo-2-arylethylidene)-3,4-dihydro-1*H*-quinoxalin-2-ones (**1a–d**) or 3-(2-oxo-2-arylethylidene)-3,4-dihydrobenzo[1,4]oxazin-2-ones (**2a–d**) (10 mmol) was added to an acetic acid/toluene (1:1) solvent mixture (30 mL). The resulting mixture is heated to slightly above boiling and turned into a yellow transparent solution. BF_3OEt (5.6 g, 50 mmol) is dropped slowly to such a solution, which immediately turns dark red. After the solution is refluxed for 5 min and slowly cooled to room temperature. The precipitated solid is filtered and successively washed by methanol and ether for several times.

4.2.1. 3-(2-Oxo-2-phenylvinyl)-1H-quinoxalinonatoboron difluoride *3a*

Orange powder in 91% yield, m.p. 313–314 °C; FT-IR (KBr): ν 1684, 1613, 1561, 1518, 1490, 1392, 1112, 1043, 753, 689 cm^{-1}; ^{1}H NMR (400 MHz, DMSO-d_6): δ 7.28 (s, 1H, CH=C), 7.33–7.34 (m, 2H, Ar–Hs), 7.49–7.54 (m, 1H, Ar–H), 7.60–7.63 (m, 2H, Ar–Hs), 7.67–7.98 (m, 1H, Ar–H), 8.11 (d, J = 7.2 Hz, 3H, Ar–Hs), 12.88 (s, 1H, NH); ^{13}C NMR (100 MHz, DMSO-d_6): δ 90.46, 115.37, 116.41, 121.37, 123.94, 126.97, 128.73, 129.27, 133.16, 133.29, 152.61, 153.26, 169.39; ^{11}B NMR (128 MHz, DMSO-d_6): δ 2.74 (t, J = 12.88 Hz); ^{19}F NMR (376 MHz, DMSO-d_6) δ −122.92 (d, J = 26.3 Hz); Found: C, 61.93; H, 3.67; N, 9.17; Calc. for $C_{16}H_{11}BF_2N_2O_2$: C, 61.74; H, 3.54; N, 9.00%.

4.2.2. 3-[2-Oxo-2-(4-methyoxyphenyl)vinyl]-1H-quinoxalinonatoboron difluoride *3b*

Carmine needle crystal in 98% yield, m.p. 283–285 °C; FT-IR (KBr): ν 1682, 1602, 1559, 1527, 1490, 1391, 1263, 1169, 1121, 824, 746, 722 cm m^{-1}; ^{1}H NMR (400 MHz, DMSO-d_6): δ 3.89 (s, 3H, OCH_3), 7.14 (d, J = 8.4 Hz, 2H, Ar–Hs), 7.18 (s, 1H, CH=C), 7.33 (d, J = 7.8 Hz, 2H, Ar–Hs), 7.46 (t, J = 7.2 Hz, 1H, Ar–H), 8.10 (d, J = 8.4 Hz, 3H, Ar–Hs), 12.78 (s, br, 1H, NH); ^{13}C NMR (100 MHz, DMSO-d_6): δ 55.80, 90.57, 114.92, 117.15, 120.88, 123.44, 123.91, 125.31, 128.15, 130.39, 144.46, 148.66, 152.12, 154.79, 164.27; ^{11}B NMR (128 MHz, DMSO-d_6): δ 2.49 (t, J = 13.43 Hz); ^{19}F

NMR (376 MHz, DMSO-d_6) δ −123.53 (d, J = 30.0 Hz); Found: C, 60.33; H, 3.69; N, 8.33; Calc. for $C_{17}H_{13}BF_2N_2O_3$: C, 59.82; H, 3.81; N, 8.21%.

4.2.3. 3-[2-Oxo-2-(4-chlorophenyl)vinyl]-1H-quinoxalinonatoboron difluoride **3c**

Red powder in 93% yield, m.p. 297–298 °C; FT-IR (KBr): ν 1686, 1615, 1581, 1562, 1527, 1484, 1421, 1388, 1116, 1093, 1052, 827, 753, 710 cm^{-1}; ^1H NMR (400 MHz, DMSO-d_6): δ 7.28 (s, 1H, CH=C), 7.35–7.37 (m, 2H, Ar–Hs), 7.51 (t, J = 7.8 Hz, 1H, Ar–H), 7.65 (d, J = 8.0 Hz, 2H, Ar–Hs), 8.13 (d, J = 8.0 Hz, 3H, Ar–Hs), 12.91 (s, 1H, NH); ^{13}C NMR (100 MHz, DMSO-d_6): δ 90.77, 116.36, 121.51, 123.75, 123.97, 128.87, 128.94, 129.10, 129.35, 130.98, 138.00, 149.03, 152.67, 167.78; ^{11}B NMR (128 MHz, DMSO-d_6): δ 2.89 (t, J = 12.45 Hz); ^{19}F NMR (376 MHz, DMSO-d_6) δ −122.88 (d, J = 26.3 Hz); Found: C, 55.79; H, 3.00; N, 8.33; Calc. for $C_{16}H_{10}BClF_2N_2O_2$: C, 55.65; H, 2.90; N, 8.12%.

4.2.4. 3-[2-Oxo-2-(4-nitrophenyl)vinyl]-1H-quinoxalinonatoboron difluoride **3d**

Dark red sheet crystal in 87% yield, m.p. 324–326 °C; FT-IR (KBr): ν 1682, 1618, 1573, 1522, 1342, 1115, 1041, 841, 767, 704 cm^{-1}; ^1H NMR (400 MHz, DMSO-d_6): δ 7.35 (dd, J = 8.0 Hz, 4.8 Hz, 2H, Ar–Hs), 7.39 (s, 1H, CH=C), 7.53 (t, J = 8.0 Hz, 1H, Ar–H), 8.13 (d, J = 8.4 Hz, 1H, Ar–H), 8.35 (s, 4H, Ar–Hs), 12.98 (s, br, 1H, NH); ^{13}C NMR (100 MHz, DMSO-d_6): δ 92.60, 116.50, 121.69, 121.88, 124.04, 124.17, 128.51, 129.51, 131.53, 137.82, 149.51, 152.87, 153.32, 165.56; ^{11}B NMR (128 MHz, DMSO-d_6): δ 2.63 (t, J = 12.90 Hz); ^{19}F NMR (376 MHz, DMSO-d_6) δ −122.48 (d, J = 26.3 Hz); Found: C, 54.88; H, 2.69; N, 12.13; Calc. for $C_{16}H_{10}BF_2N_3O_4$: C, 53.93; H, 2.81; N, 11.80%.

4.2.5. 3-(2-Oxo-2-phenyl)vinyl)benzo[1,4]-oxazinonatoboron difluoride **4a**

Red powder in 92% yield, m.p. 251–253 °C; FT-IR (KBr): ν 1760, 1602, 1562, 1535, 1469, 1402, 1363, 1110, 1050, 753, 692 cm^{-1}; ^1H NMR (400 MHz, DMSO-d_6): δ 7.23 (s, 1H, CH=C), 7.41–7.49 (m, 3H, Ar–Hs), 7.62 (t, J = 7.6 Hz, 2H, Ar–Hs), 7.72 (t, J = 7.8 Hz, 1H, Ar–h), 7.99 (d, J = 8.0 Hz, 1H, Ar–H), 8.18 (d, J = 7.8 Hz, 2H, Ar–Hs); ^{13}C NMR (100 MHz, DMSO-d_6): δ 91.45, 117.25, 121.12, 123.26, 125.39, 127.71, 128.86, 129.38, 131.69, 133.99, 144.84, 149.57, 153.33, 171.79; ^{11}B NMR (128 MHz, DMSO-d_6): δ 2.75 (t, J = 13.13 Hz); ^{19}F NMR (376 MHz, DMSO-d_6) δ −123.35 (d, J = 26.3 Hz); Found: C, 62.13; H, 3.33; N, 4.33; Calc. for $C_{16}H_{10}BF_2NO_3$: C, 61.54; H, 3.21; N, 4.49%.

4.2.6. 3-[2-Oxo-2-(4-methyoxyphenyl)vinyl]benzo[1,4]-oxazinonatoboron difluoride **4b**

Rosy needle crystal in 99% yield, m.p. 236–238 °C; FT-IR (KBr): ν 1755, 1599, 1560, 1537, 1511, 1467, 1364, 1270, 1174, 1127, 1048, 839, 819, 751 cm^{-1}; ^1H NMR (400 MHz, DMSO-d_6): δ 3.91 (s, 3H, OCH_3), 7.14 (s, 2H, Ar–Hs), 7.16 (s, 1H, CH=C), 7.38–7.44 (m, 3H, Ar–Hs), 7.95 (d, J = 7.8 Hz, 1H, Ar–H), 8.17 (d, J = 8.8 Hz, 2H, Ar–Hs); ^{13}C NMR (100 MHz, DMSO-d_6): δ 55.77, 90.49, 114.89, 117.14, 120.73, 123.42, 123.85, 125.30, 128.14, 130.38, 144.44, 149.73, 155.63, 164.23, 172.11; ^{11}B NMR (128 MHz, DMSO-d_6): δ 2.64 (t, J = 12.88 Hz); ^{19}F NMR (376 MHz, DMSO-d_6) δ −124.02 (d, J = 30.0 Hz); Found: C, 60.77; H, 3.62; N, 4.23; Calc. for $C_{17}H_{12}BF_2NO_4$: C, 59.65; H, 3.51; N, 4.09%.

4.2.7. 3-[2-Oxo-2-(4-chlorophenyl)vinyl]benzo[1,4]-oxazinonatoboron difluoride **4c**

Orange powder in 95% yield, m.p. 243–245 °C; FT-IR (KBr): ν 1759, 1603, 1566, 1535, 1485, 1465, 1421, 1367, 1125, 1094, 823, 746 cm^{-1}; ^1H NMR (400 MHz, DMSO-d_6): δ 7.21 (s, 1H, CH=C), 7.41–7.54 (m, 3H, Ar–Hs), 7.67 (d, J = 8.4 Hz, 2H, Ar–Hs), 8.00 (dd, J = 8.0 Hz, 8.0 Hz, 1H, Ar–H), 8.20 (d, J = 8.4 Hz, 2H, Ar–Hs); ^{13}C NMR (100 MHz, DMSO-d_6): δ 92.74, 117.26, 117.77, 121.72, 125.93, 129.97, 130.03, 131.05, 139.25, 141.71, 145.42, 150.15, 153.73, 170.83; ^{11}B NMR (128 MHz, DMSO-d_6): δ 2.61 (t, J = 11.98 Hz); ^{19}F NMR (376 MHz, DMSO-d_6) δ −123.27 (d, J = 26.3 Hz); Found: C, 55.96; H, 2.67; N, 3.96; Calc. for $C_{16}H_9BClF_2NO_3$: C, 55.49; H, 2.60; N, 4.05%.

4.2.8. 3-[2-Oxo-2-(4-nitrophenyl)vinyl]benzo[1,4]-oxazinonatoboron difluoride **4d**

Scarlet sheet crystal in 83% yield, m.p. 257–259 °C; FT-IR (KBr): ν 1759, 1602, 1571, 1532, 1344, 1126, 1050, 845, 759, 702 cm^{-1}; ^1H NMR (400 MHz, DMSO-d_6): δ 7.32 (s, 1H, CH=C), 7.40–7.46 (m, 2H, Ar–Hs), 7.52 (t, J = 7.8 Hz, 1H, Ar–H), 7.99 (d, J = 8.0 Hz, 1H, Ar–H), 8.33 (d, J = 8.8 Hz, 2H, Ar–Hs), 8.39 (d, J = 8.8 Hz, 2H, Ar–Hs); ^{13}C NMR (100 MHz, DMSO-d_6): δ 92.97, 118.43, 123.77, 124.13, 124.56, 126.37, 129.06, 131.76, 133.82, 139.10, 151.53, 154.39, 156.67, 172.81; ^{11}B NMR (128 MHz, DMSO-d_6): δ 2.40 (t, J = 13.35 Hz); ^{19}F NMR (376 MHz, DMSO-d_6) δ −122.85 (d, J = 26.3 Hz); Found: C, 54.13; H, 2.44; N, 7.99; Calc. for $C_{16}H_9BF_2N_2O_5$: C, 53.78; H, 2.52; N, 7.84%.

4.3. X-ray data collection, structure determination and refinement

A red single crystal (0.40 mm × 0.20 mm × 0.11 mm) is attached to a glass fiber and mounted on a Rigaku RAXIS-RAPID X-ray diffractometer equipped with a graphite monochromated Mo Kα (λ = 0.71073 Å) radiation source and an IP detector. Absorption correction is performed by multi-scan based on symmetry-equivalent and repeated reflections. The structure is solved by direct methods using SHELXS-97 and refined by a full matrix least-squares calculation on F^2 using SHELXL-97. Molecular graphics are produced using ORTEP-3. Non-hydrogen atoms are refined anisotropically; all H atoms are then constrained to an ideal geometry and have not been refined.

Supplemental material

Crystallographic data, tables of atomic coordinates and thermal parameters, and full lists of bond lengths and angles

have been deposited with the Cambridge Crystallographic Data Center (CCDC), No. 652824. Copies of this information can be obtained free of charge from The Director, CCDC, 12 Union Road, Cambridge CB2 1EZ, UK (fax: +44-1223-336-033; e-mail: deposit@ccdc.cam.ac.uk or http://www.ccdc.cam.ac.uk)

Acknowledgments

We are grateful for the financial support from the Natural Science Foundation of Zhejiang Province (R405465) and PCSIRT (No. 0654).

References

[1] P. Oleynik, Y. Ishihara, G. Cosa, J. Am. Chem. Soc. 129 (2007) 1842–1843.
[2] T. Yogo, Y. Urano, Y. Ishitsuka, F. Maniwa, T. Nagano, J. Am. Chem. Soc. 127 (2005) 12162–12163.
[3] Z. Li, E. Mintzer, R. Bittman, J. Org. Chem. 71 (2006) 1718–1721.
[4] M. Baruah, W. Qin, N. Basaric, W.M. DeBorggraeve, N. Boens, J. Org. Chem. 70 (2005) 4152–4157.
[5] D. Rhode, C.J. Yan, L.J. Wan, Langmuir 22 (2006) 4750–4757.
[6] B. Bomercq, C. Grasso, J.L. Maldonado, M. Halik, S. Barlow, S.R. Marder, B. Kippelen, J. Phys. Chem. B 108 (2004) 8641–8651.
[7] C. Risko, E. Zojer, P. Brocorens, S.R. Marder, J.L. Bredas, Chem. Phys. 313 (2005) 151–157.
[8] V.F. Traven, A.V. Manaev, T.A. Chibisova, J. Electron Spectrosc. Relat. Phenom. 149 (2005) 6–10.
[9] K. Itoh, K. Okazaki, M. Fujimoto, Aust. J. Chem. 56 (2003) 1209–1214.
[10] K. Itoh, K. Okazaki, Y. Toyotomi, New J. Chem. 26 (2002) 1070–1075.
[11] K. Itoh, K. Okazaki, A. Sera, Y.L. Chow, J. Chem. Soc. Chem. Commun. (1992) 1608–1609.
[12] M. Xia, S.Q. Ge, X.S. Li, Acta Crystallogr. Sect. E 62 (2006) 2625–2626.
[13] Y. Iwanami, T. Seki, T. Inagaki, Bull. Chem. Soc. Jpn. 44 (1971) 1316–1321.
[14] D. TrongOn, P.N. Joshi, G. Lemay, S. Kaliaguine, Stud. Surf. Sci. Catal. 97 (1995) 543–549.
[15] N.N. Greenward, J. Walker, J. Chem. Soc. Chem. Commun. (1961) 959–961.